Extremely large magnetoresistance in high-mobility math xmlns="http://www.w3.org/1998/Math/MathML">msub>mi mathvariant="normal">SrNbO/mi>mn>3/mn>/msub>mo >//mo>msub>mi mathvariant="normal">SrTiO/mi> mn>3/mn>/msub>/math> heterostructures

Jie Zhang, Jong Mok Ok, Yun-Yi Pai, Jason Lapano, Elizabeth Skoropata, Alessandro R. Mazza, Haoxiang Li, Amanda Huon, Sangmoon Yoon, Benjamin Lawrie, Matthew Brahlek, T. Zac Ward, Gyula Eres, H. Miao, and Ho Nyung Lee

Phys. Rev. B **104**, L161404 — Published 13 October 2021

DOI: 10.1103/PhysRevB.104.L161404

The Nature of Extremely Large Magnetoresistance in High Mobility $SrNbO_3/SrTiO_3$ Heterostructures

Jie Zhang*, Jong Mok Ok*, Yun-Yi Pai, Jason Lapano, Elizabeth Skoropata, Alessandro R. Mazza, Haoxiang Li, Amanda Huon, Sangmoon Yoon, Benjamin Lawrie, Matthew Brahlek, T. Zac Ward, Gyula Eres, H. Miao, Ho Nyung Lee#

Material Science and Technology Division, Oak Ridge National Laboratory, Oak Ridge, Tennessee 37830, USA

(Dated: September 20, 2021)

Extremely large linear magnetoresistance (LMR) is a ubiquitous phenomenon emerging from topological Dirac and Weyl semimetals. However, the connection between LMR and non-trivial topology is under extensive debate. In this letter, by precisely controlling the thickness of $SrNbO_3$ thin films grown on $SrTiO_3$ substrates, we observe LMR over a large carrier density range with a MR as high as $150,000\%$ at carrier density $n \sim 10^{21}\,\mathrm{cm}^{-3}$, far away from the quantum limit regime. The temperature, magnetic field and carrier density-dependent LMR in $SrNbO_3/SrTiO_3$ heterostructures provides compelling evidence of a mobility-driven LMR in coherent electronic systems. Our results uncover the general principle of LMR and shed light on proper categorization of transport properties in topological and correlated materials.

Electrical resistance in response to an external magnetic field, i.e. magnetoresistance (MR), encodes information about low-energy electronic excitations that are fundamentally tied to the quasi-particle dynamics in quantum materials [1–3]. For conventional nonmagnetic metals, MR is quadratic in low field and quickly saturates to a constant value [4, 5]. Deviation from this behavior, including the extremely large MR, is usually an indication of non-trivial low-energy electronic structure, such as perfectly compensated electron/hole Fermi surfaces (Fig. 1(a)) [6–11] and strong inhomogeneity-induced charge/mobility fluctuation (Fig. 1(c)) [12, 13]. In the last few years, the extremely large MR with linear field dependence (LMR, exclusively refer to linear magnetoresistance in this manuscript), has been widely observed in topological Dirac and Weyl semimetals [14–22], suggesting an intimate correlation between topological quasi-particles and LMR, as illustrated in Fig. 1(b). This picture, however, was challenged by a semiclassical guiding center model (Fig. 1(d)) [23] in order to address the discrepancy between the massive carrier numbers in some materials and the lowest Landau level occupation required by the quantum MR mechanism [24]. Releasing conditions on band structure, LMR in the guiding center model is a direct consequence of long electron mean free path and high mobility. While the high mobility condition is usually satisfied in topological semimetals with dilute carriers due to linear dispersion, they can, in principle, be realized in ultra-pure metals without topological quasi-particles near the Fermi level. To uncover the nature of LMR, it is critical to have an ideal material platform, where LMR can be realized in a wide carrier density range. Here we demonstrate that the $SrNbO_3/SrTiO_3$ heterostructure is such a system. By tuning the carrier density through precise control of the film thickness, we find LMR exists in a wide range of carrier density and the magnitude of LMR is related to carrier mobility μ and the Hall angle θ_H. The $MR = \Delta\rho/\rho_0 = \rho(H)$ as high as $150,000\%$ is achieved far away from the semimetal regime with carrier density $\sim 10^{21}\,\mathrm{cm}^{-3}$. Our results establish the general relation between LMR, mobility, Hall angle, and thus support a more general guiding center mechanism.

$SrNbO_3$ has a simple ABO_3 perovskite structure [25–27]. Despite the difficulty of bulk single crystal synthesis, epitaxial growth at a relatively low temperature with no impurity phase or Sr vacancies can be achieved by pulsed laser deposition (PLD) [26, 28]. We grow high-quality single crystal $SrNbO_3$ films on $SrTiO_3$ substrates by PLD. The highest mobility is obtained at optimal thickness $d^* = 4.8\,\mathrm{nm}$ with a fully-strained lattice and a large carrier density ($n \sim 10^{21}\,\mathrm{cm}^{-3}$), providing a versatile platform to study LMR in a high density regime. X-ray diffraction demonstrates that films are strained up to 15 nm as shown in Supplemental Material. Transport measurements are performed in a physical property measurement system (Quantum Design) with Van der Pauw geometry. Metallicity of the heterostructure persists down to 2.0 nm film at low temperatures. The exceptionally high residual resistivity ratio $RRR = \rho(300K)/\rho(2K) \sim 10,000$ indicates the high sample quality [29], as shown the inset of Fig. 1(e).

Figure 1(e) displays an LMR up to $150,000\%$ at 14 T and 2 K on a strained $SrNbO_3/SrTiO_3$ heterostructure. This is comparable with that from well-known Dirac/Weyl semimetals [14, 15, 19, 21, 28, 30–34]. A two-band model fitting of the Hall resistivity shows electron- and hole-type carriers, both of which are on the order of $10^{21}\,\mathrm{cm}^{-3}$. The carrier type is consistent with previous angle-resolved photoemission spectroscopy [25] as well as density functional theory [27], that show two smaller electron pockets and a larger jungle-gym Fermi surface, all centered at the Γ-point.(See Supplemental Materials, also, [35–37] therein)

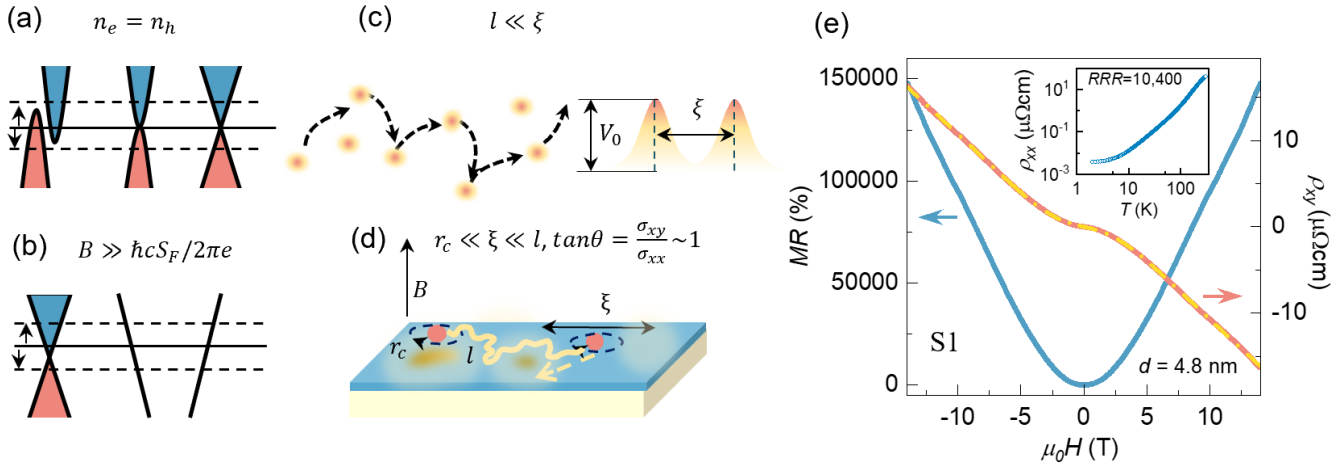

Figure 1. Schematics of mechanisms to induce large magnetoresistance: (a) Extreme quantum limit in topological semimetals. S_F is the size of the Fermi surface. (b) Perfect electron/hole compensation. In scenarios (a) and (b), the LMR is expected to disappear when chemical potential (dashed lines) is tuned away from the "ideal condition" (solid line). (c) Strong-disorder limit where $eV_0 \gg \mu_0$. V_0 is the average potential height of disorder, μ_0 is the chemical potential. Yellow islands represent local disorder and black arrows denote electron trajectories due to random scattering. (d) Guiding center model in the weak-disorder limit $eV_0 \ll \mu_0$. Red dots represent charge carriers and black circles with arrows indicate cyclotron orbits. Yellow regions and bright yellow line denote disorder potentials and electrons squeezed trajectory. (e) Field dependence of MR (solid blue) and Hall resistivity (solid orange) in sample 1 (S1) (4.8 nm) at 2 K displaying an LMR up to 150,000% at 14 T. The nonlinear Hall curve fitting (dash yellow) indicates an electron/hole two-carrier behavior.

The high but yet not perfectly compensated carrier density proves that LMR can be realized in a system far from the semimetal regime, where carrier density is typically below $10^{18}\,\mathrm{cm}^{-3}$ [6, 10, 11, 15].

Carrier concentration in our heterostructures can be tuned over two orders of magnitude by varying film thicknesses (See Supplemental Material). This allows us to track the interplay between LMR and evolution of the Fermi surface curvature. Figures 2(b,d,f) show Hall resistivity of samples S2, S3 and S4 with different thickness. The carrier densities are extracted by employing a two-carrier model fitting (Supplemental Material), showing a transition from two electron bands (Fig. 2(b)) to electron and hole-like bands (Fig. 2(d,f)) with increasing thickness. Fig. 2(a,c,e) present MR in corresponding samples with different carrier densities. While the magnitude of MR varies, they all display linear dependence at high field, as validated by taking the first derivative of resistivity with respect to the magnetic field (orange curves). The observation of LMR over a wide carrier concentration demonstrates that LMR is not a unique property of topological semimetals. This is our first main experimental finding.

The widely observed LMR over a wide range of carrier concentrations in high quality $SrNbO_3/SrTiO_3$ heterostructures thus points to a more general mechanism for the nature of LMR. As we show below, our observations are quantitatively consistent with the semiclassical guiding center model, where electrons with $l \gg \xi \gg r_c$ travel coherently across many weakly-disordered potentials before scattering (l is the mean free path, ξ is the characteristic length of disorder and r_c is the cyclotron radius).

We first look at one of the most important features of the guiding center model, *i.e.*, $1/B^*$ scales linearly with the averaged mobility $\langle\mu\rangle$ [23, 38]. Here B^* is defined as linear-to-saturation crossover field in $\mathrm{d}MR/\mathrm{d}B$ as displayed in the inset of Fig. 2(g). The extracted $1/B^*$ (orange) and $<\mu>$ (cyan) from S1 are shown in Fig. 2(h). The same temperature dependence of these two quantities strongly supports a mobility-driven LMR. We then move to another key feature of the guiding center model, which predicts that the tangent of the Hall angle

$$\tan\theta_H = \frac{\sigma_{xy}}{\sigma_{xx}}$$

saturates to a constant value at high magnetic field. This can be understood by expressing the longitudinal resistivity as a function of the longitudinal conductivity and Hall angle:

$$\rho_{xx} = \frac{\sigma_{xx}}{\sigma_{xx}^2 + \sigma_{xy}^2} = \frac{G}{\sigma_{xy}} = \frac{1}{\sigma_{xx}(1+\tan^2\theta_H)} \qquad (1)$$

where $G(\tan\theta_H) = \tan\theta_H/(1+\tan^2\theta_H)$ [23]. For a high field-saturated Hall angle, MR can, in principle, be enhanced either by maximizing G or minimizing σ_{xy}. In the high-field limit ($B \gg 1/\mu_e, 1/\mu_h$), $\sigma_{xy} = e(n_e - n_h)/B$ [39]. While extremely large MR can be easily realized

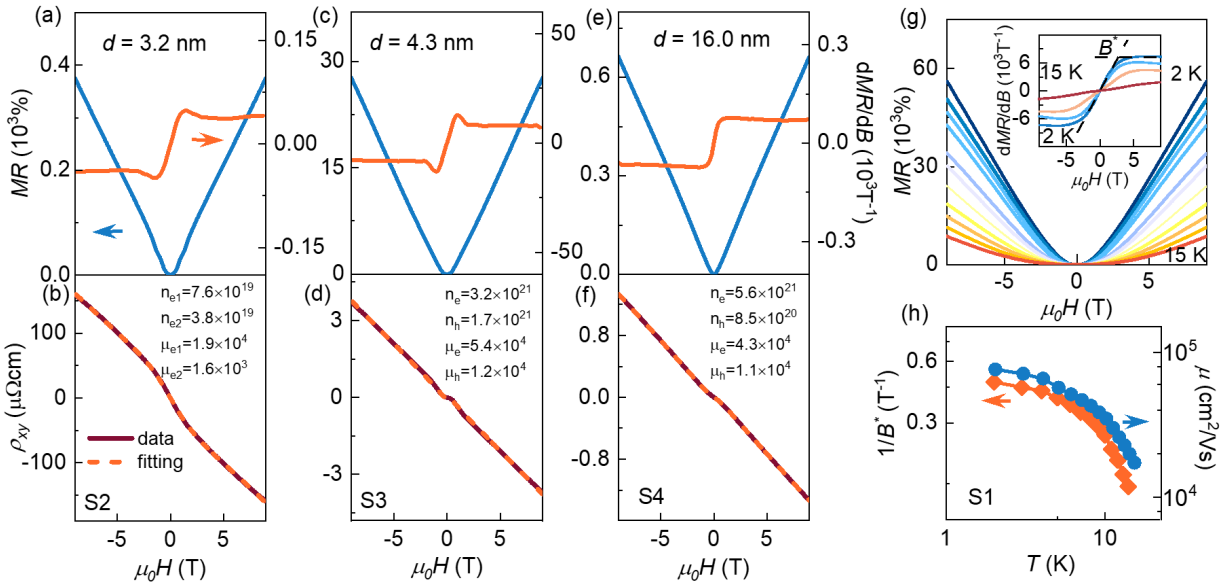

Figure 2. (a-f) MR (blue), dMR/dB (orange) and Hall resistivity (solid purple) and two-carrier fitting (dashed orange) curves on three representative samples S2 (3.2 nm), S3 (4.3 nm), S4 (16.0 nm) with different carrier concentration. (g) Field dependence of MR in S1 at selective temperatures displaying a transition from LMR to quadratic dependence at higher temperatures. Inset is the first derivative of MR showing saturation at 2 K (LMR) and linear dependence at 15 K (quadratic MR). The linear to saturation crossover field is denoted as B^*. (h) Consistent temperature dependence of $1/B^*$ and mobility indicate an underlying relation between them.

in compensated materials with $n_e = n_h$, it increases quadratically with B [6, 7]. The LMR can be achieved, according to Eq. 1, for uncompensated cases, under constant G. Notably, the maximum value of G is achieved when $\tan\theta_H \sim 1$. This simple mathematical observation is the most specific and compelling evidence in favor of the guiding center model.

To prove these predictions, in Fig. 3(a,b), we show ρ_{xx}, ρ_{xy} and the extracted $\tan\theta_H$ as a function of temperature and magnetic field. The LMR-induced resistivity upturn shown in the inset of Fig. 3(a) has a small onset field. However, as the applied magnetic field increases, both longitudinal resistivity (solid) and Hall resistivity (dashed) start to decrease at lower temperatures, exhibiting a peak around 10 K (the origin of such anomalous temperature behavior is discussed in the Supplemental Material). Remarkably, as displayed in Fig. 3(b), $\tan\theta_H$ saturates above 5 T to a value which monotonically increases with temperature and crosses unity at 9 K (Fig. 3(c)). Most importantly, we find that the highest ρ_{xx} is observed near $\tan\theta_H \sim 1$, fully consistent with the guiding center model.

Finally, we compare experimentally determined $\rho_{xx}(9\,\mathrm{T})$ with theoretical prediction. Following the guiding center model [23], LMR is estimated as:

$$\rho_{xx}(B) \sim \frac{\mu}{10^4} B(T) G(\tan\theta_H) \qquad (2)$$

As we show in Fig. 3(d), the good agreement between experiment (cyan) and theory (yellow), once again support the guiding center model as the origin of LMR.

The quantitative agreement between our observations in $SrNbO_3/SrTiO_3$ heterostructures and the guiding center model provides a solid foundation for the general principle of LMR in quantum materials. Fig. 4 surveys a broad class of LMR materials, including semimetals [14–17, 19, 21, 42], normal metals [40] and topological trivial/nontrivial systems [18, 34, 43]. Materials with quadratic magnetic field dependence are not presented here. Carrier concentration, mobility under a typical condition of 2 K, 9 T and LMR are gathered . Here the dashed arrow in Fig. 4(a) is provided as a guide to the eye on the positive relation between LMR and carrier mobility. In contrast to the mobility dependence, we do not observe any obvious connection between LMR and carrier density in Fig. 4(b). These results strongly support the guiding center model where high mobility is a common thread and hints at a generic origin of all LMR materials. This constitutes the second main result of the present work.

While in topological semimetals, the high carrier mobility naturally arises from the linearly dispersive bands, the observed high mobility in the $SrNbO_3/SrTiO_3$ heterostructures is worth a discussion. At optimized film thickness, the electron mobility ($80\,000\,\mathrm{cm}^2/\mathrm{Vs}$ at 2 K) is over an order of magnitude higher than doped-$SrTiO_3$ single crystals [44–46]. Similar galvanomagnetic observations have been reported in other $SrTiO_3$-based systems, like γ−$Al_2O_3/SrTiO_3$ [47], oxygen-deficient $SrTiO_3$ [44]

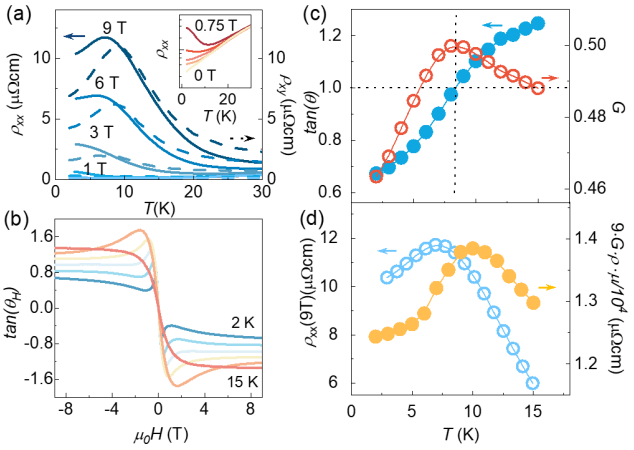

Figure 3. Transport properties of S1. (a) Temperature dependence of longitudinal (solid) and Hall resistivity (dashed) at selected fields displaying the anomalous behavior below 10 K. Inset is the temperature dependence of longitudinal resistivity at low fields showing an upturn above 0.5 T. (b) Field dependence of $\tan\theta_H$ at selected temperatures. Saturation of $\tan\theta_H$ is demonstrated by the flat curves above 5 T. (c) Temperature dependence of the saturated $\tan\theta_H$ at 9 T taken from (b) and corresponding G evaluated from eqn.(1). $\tan\theta_H$ crosses unity at 9 K and the peak indicates G reach a maximum when $\tan\theta_H = 1$. (d) Temperature dependence of longitudinal resistivity at 9 T, $\rho_{xx}(9T)$ and $9{\cdot}\rho_0{\cdot}G(\theta){\cdot}\mu/10^4$ (calculated from extracted values), exhibiting qualitative agreement between estimation from eqn.(2) and the experimental result.

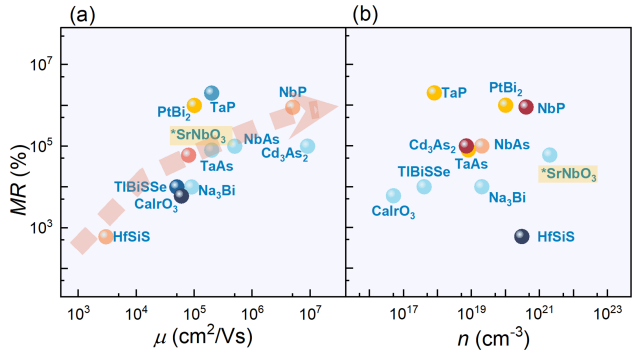

Figure 4. MR as function of (a) mobility and (b) carrier density from various materials exhibiting large LMR with typical conditions of 2 K and 9 T. Data are extracted from [14–22, 34, 40–43]. Colors are coded with carrier density in (a) and mobility in (b) from low (blue) to high (red). *$SrNbO_3$ here is the $SrNbO_3/SrTiO_3$ heterostructure. Note the parameters are extracted from the dominant carrier type for multi-carrier materials.

and $Sr_2CrWO_6/SrTiO_3$ [48]. The magnitude of MR in these works is found to be positively related to sample mobility and the observed large MR is attributed to spatial inhomogeneity [44]. In these systems, transport properties are highly dependent on the nature of the interface (e.g. strain, charge transfer) and carrier density is usually low or not tunable. The exceptionally high RRR in $SrNbO_3/SrTiO_3$ heterostructures indicates a low defect concentration with optimized screening that occurs at low temperatures. The carrier mobility in the bipolar (electron-hole) thickness regime is found to be an order of magnitude higher than the thin (electron-electron) and thick (single electron) regimes (see Supplemental Material). While the microscopic origin of such high mobility may require further study, we suspect that metallic screening from the film together with the exceptionally large dielectric screening of the $SrTiO_3$ substrate may play a crucial role [29, 49].

In summary, our observations in $SrNbO_3/SrTiO_3$ heterostructures with carrier concentration vary with thickness, over several orders of magnitude uncovers the nature of LMR and sheds light on proper categorization of transport properties in topological and correlated materials.

This work was sponsored by the U. S. Department of Energy, Office of Science, Basic Energy Sciences, Materials Sciences and Engineering Division. J.Z. and J.O. contributed equally to this work.

[1] X.-L. Qi and S.-C. Zhang, Rev. Mod. Phys. **83**, 1057 (2011).
[2] K. von Klitzing, Annual Review of Condensed Matter Physics **8**, 13 (2017), https://doi.org/10.1146/annurev-conmatphys-031016-025148.
[3] C.-L. Zhang, C. M. Wang, Z. Yuan, X. Xu, G. Wang, C.-C. Lee, L. Pi, C. Xi, H. Lin, N. Harrison, H.-Z. Lu, J. Zhang, and S. Jia, Nature Communications **10**, 1028 (2019).
[4] A. B. Pippard, *Magnetoresistance in Metals* (Cambridge University Press, 1989).
[5] J. Hu and T. F. Rosenbaum, Nature Materials **7**, 697 (2008).
[6] F. Y. Yang, K. Liu, K. Hong, D. H. Reich, P. C. Searson, and C. L. Chien, Science **284**, 1335 (1999).
[7] M. N. Ali, J. Xiong, S. Flynn, J. Tao, Q. D. Gibson, L. M. Schoop, T. Liang, N. Haldolaarachchige, M. Hirschberger, N. P. Ong, and R. J. Cava, Nature **514**, 205 (2014).
[8] O. Pavlosiuk, P. Swatek, D. Kaczorowski, and P. Wiśniewski, Phys. Rev. B **97**, 235132 (2018).
[9] L. Zhao, Q. Xu, X. Wang, J. He, J. Li, H. Yang, Y. Long, D. Chen, H. Liang, C. Li, M. Xue, J. Li, Z. Ren, L. Lu, H. Weng, Z. Fang, X. Dai, and G. Chen, Phys. Rev. B **95**, 115119 (2017).
[10] M. Matin, R. Mondal, N. Barman, A. Thamizhavel, and S. K. Dhar, Phys. Rev. B **97**, 205130 (2018).
[11] Z. Yuan, H. Lu, Y. Liu, J. Wang, and S. Jia, Phys. Rev. B **93**, 184405 (2016).
[12] R. Xu, A. Husmann, T. F. Rosenbaum, M.-L. Saboungi, J. E. Enderby, and P. B. Littlewood, Nature **390**, 57 (1997).
[13] M. M. Parish and P. B. Littlewood, Phys. Rev. B **72**, 094417 (2005).

[14] T. Liang, Q. Gibson, M. N. Ali, M. Liu, R. J. Cava, and N. P. Ong, Nature Materials **14**, 280 (2015).

[15] J. Xiong, S. Kushwaha, J. Krizan, T. Liang, R. J. Cava, and N. P. Ong, Europhysics Letters **114**, 27002 (2016).

[16] X. Huang, L. Zhao, Y. Long, P. Wang, D. Chen, Z. Yang, H. Liang, M. Xue, H. Weng, Z. Fang, X. Dai, and G. Chen, Phys. Rev. X **5**, 031023 (2015).

[17] J. Fujioka, R. Yamada, M. Kawamura, S. Sakai, M. Hirayama, R. Arita, T. Okawa, D. Hashizume, M. Hoshino, and Y. Tokura, Nature Communications **10**, 362 (2019).

[18] N. Kumar, K. Manna, Y. Qi, S.-C. Wu, L. Wang, B. Yan, C. Felser, and C. Shekhar, Phys. Rev. B **95**, 121109 (2017).

[19] M. Novak, S. Sasaki, K. Segawa, and Y. Ando, Phys. Rev. B **91**, 041203 (2015).

[20] C.-L. Zhang, S.-Y. Xu, C. M. Wang, Z. Lin, Z. Z. Du, C. Guo, C.-C. Lee, H. Lu, Y. Feng, S.-M. Huang, G. Chang, C.-H. Hsu, H. Liu, H. Lin, L. Li, C. Zhang, J. Zhang, X.-C. Xie, T. Neupert, M. Z. Hasan, H.-Z. Lu, J. Wang, and S. Jia, Nature Physics **13**, 979 (2017).

[21] W. Gao, N. Hao, F.-W. Zheng, W. Ning, M. Wu, X. Zhu, G. Zheng, J. Zhang, J. Lu, H. Zhang, C. Xi, J. Yang, H. Du, P. Zhang, Y. Zhang, and M. Tian, Phys. Rev. Lett. **118**, 256601 (2017).

[22] C. Shekhar, A. K. Nayak, Y. Sun, M. Schmidt, M. Nicklas, I. Leermakers, U. Zeitler, Y. Skourski, J. Wosnitza, Z. Liu, Y. Chen, W. Schnelle, H. Borrmann, Y. Grin, C. Felser, and B. Yan, Nature Physics **11**, 645 (2015).

[23] J. C. W. Song, G. Refael, and P. A. Lee, Phys. Rev. B **92**, 180204 (2015).

[24] A. A. Abrikosov, Phys. Rev. B **58**, 2788 (1998).

[25] C. Bigi, P. Orgiani, J. Sławińska, J. Fujii, J. T. Irvine, S. Picozzi, G. Panaccione, I. Vobornik, G. Rossi, D. Payne, and F. Borgatti, Phys. Rev. Materials **4**, 025006 (2020).

[26] D. Oka, Y. Hirose, S. Nakao, T. Fukumura, and T. Hasegawa, Phys. Rev. B **92**, 205102 (2015).

[27] Y. Park, J. Roth, D. Oka, Y. Hirose, T. Hasegawa, A. Paul, A. Pogrebnyakov, V. Gopalan, T. Birol, and R. Engel-Herbert, Communications Physics **3**, 102 (2020).

[28] J. M. O. et. al. Correlated Oxide Dirac Semimetal in the Extreme Quantum Limit (under review), .

[29] E. Mikheev, B. Himmetoglu, A. P. Kajdos, P. Moetakef, T. A. Cain, C. G. Van de Walle, and S. Stemmer, Applied Physics Letters **106**, 062102 (2015).

[30] N. Kumar, Y. Sun, N. Xu, K. Manna, M. Yao, V. Süss, I. Leermakers, O. Young, T. Förster, M. Schmidt, H. Borrmann, B. Yan, U. Zeitler, M. Shi, C. Felser, and C. Shekhar, Nature Communications **8**, 1642 (2017).

[31] O. Pavlosiuk and D. Kaczorowski, Scientific Reports **8**, 11297 (2018).

[32] N. Kumar, C. Shekhar, S.-C. Wu, I. Leermakers, O. Young, U. Zeitler, B. Yan, and C. Felser, Phys. Rev. B **93**, 241106 (2016).

[33] Y. Li, L. Li, J. Wang, T. Wang, X. Xu, C. Xi, C. Cao, and J. Dai, Phys. Rev. B **94**, 121115 (2016).

[34] M. N. Ali, L. M. Schoop, C. Garg, J. M. Lippmann, E. Lara, B. Lotsch, and S. S. P. Parkin, Science Advances **2** (2016), 10.1126/sciadv.1601742.

[35] M. Kaveh and N. Wiser, Adv. Phys. **33**, 257372 (1984).

[36] N. P. Ong, Phys. Rev. B **43**, 193 (1991).

[37] J. S. Kim, S. S. A. Seo, M. F. Chisholm, R. K. Kremer, H.-U. Habermeier, B. Keimer, and H. N. Lee, Phys. Rev. B **82**, 201407 (2010).

[38] A. Narayanan, M. D. Watson, S. F. Blake, N. Bruyant, L. Drigo, Y. L. Chen, D. Prabhakaran, B. Yan, C. Felser, T. Kong, P. C. Canfield, and A. I. Coldea, Phys. Rev. Lett. **114**, 117201 (2015).

[39] C. Kittel, *Quantum Theory of Solids* (New York : Wiley, 1963).

[40] I. A. Leahy, Y.-P. Lin, P. E. Siegfried, A. C. Treglia, J. C. W. Song, R. M. Nandkishore, and M. Lee, Proceedings of the National Academy of Sciences **115**, 10570 (2018).

[41] B. Fauqué, X. Yang, W. Tabis, M. Shen, Z. Zhu, C. Proust, Y. Fuseya, and K. Behnia, Phys. Rev. Materials **2**, 114201 (2018).

[42] C. Shekhar, V. Sss, and M. Schmidt, "Mobility induced unsaturated high linear magnetoresistance in transition-metal monopnictides weyl semimetals," (2016), arXiv:1606.06649.

[43] M. G. Vergniory, L. Elcoro, C. Felser, N. Regnault, B. A. Bernevig, and Z. Wang, Nature **566**, 480 (2019).

[44] A. Bhattacharya, B. Skinner, G. Khalsa, and A. V. Suslov, Nature Communications **7**, 12974 (2016).

[45] A. Verma, A. P. Kajdos, T. A. Cain, S. Stemmer, and D. Jena, Phys. Rev. Lett. **112**, 216601 (2014).

[46] S. Kobayashi, Y. Mizumukai, T. Ohnishi, N. Shibata, Y. Ikuhara, and T. Yamamoto, ACS Nano **9**, 10769 (2015).

[47] Y. Z. Chen, N. Bovet, F. Trier, D. V. Christensen, F. M. Qu, N. H. Andersen, T. Kasama, W. Zhang, R. Giraud, J. Dufouleur, T. S. Jespersen, J. R. Sun, A. Smith, J. Nygård, L. Lu, B. Büchner, B. G. Shen, S. Linderoth, and N. Pryds, Nature Communications **4**, 1371 (2013).

[48] J. Zhang, W.-J. Ji, J. Xu, X.-Y. Geng, J. Zhou, Z.-B. Gu, S.-H. Yao, and S.-T. Zhang, Science Advances **3** (2017), 10.1126/sciadv.1701473.

[49] H. Weaver, Journal of Physics and Chemistry of Solids **11**, 274 (1959).